JGR Oceans

RESEARCH ARTICLE
10.1029/2021JC018122

Special Section:
The Arctic: An AGU Joint Special Collection

Observed Changes in the Arctic Freshwater Outflow in Fram Strait

T. Karpouzoglou[1,2], L. de Steur[1], L. H. Smedsrud[2], and H. Sumata[1]

[1]Norwegian Polar Institute, Tromsø, Norway, [2]Geophysical Institute, University of Bergen, Bergen, Norway

Key Points:

- Mean fresh water transport of the East Greenland Current in Fram Strait decreased after 2015 due to weaker velocity and increased salinity
- Both the vertical as well as the lateral extent of the Polar Water has decreased relative to 2003–2015
- Large fresh water transport from the Arctic in 2017 formed an exception to the Atlantification trend observed in the western Fram Strait

Supporting Information:

Supporting Information may be found in the online version of this article.

Correspondence to:

T. Karpouzoglou,
thodoris.karpouzoglou@npolar.no

Citation:

Karpouzoglou, T., de Steur, L., Smedsrud, L. H., & Sumata, H. (2022). Observed changes in the Arctic freshwater outflow in Fram Strait. *Journal of Geophysical Research: Oceans*, *127*, e2021JC018122. https://doi.org/10.1029/2021JC018122

Received 11 OCT 2021
Accepted 14 FEB 2022

Abstract

We have updated time series of liquid fresh water transport (FWT) in the East Greenland Current (EGC) in the western Fram Strait with mooring observations since 2015. Novel data have been used to correct earlier estimates when instrument coverage was lower. The updated FWT (reference salinity 34.9) shows that the increased export between 2010 and 2015 has not continued, but FWT has decreased to pre-2009 levels. Salt transport independent of a reference salinity is shown not to be sensitive to salinity changes. Between 2015 and 2019, the FWT in the Polar Water (PW) decreased to an average of 59.9 (±4.5) mSV, 15% less than the 2003–2019 long-term mean, however, high FWT events occurred in 2017. The overall decrease is related to a slowdown of the EGC, partly attributed to a decrease of the zonal density gradient, due to stronger salinification of the halocline waters ($26.5 < \sigma_\theta < 27.7$ kg/m^3) over the shelf. This salinification counterbalances the freshening of the surface layer ($\sigma_\theta < 26.5$ kg/m^3) and the fresh water content decreases. Our results show changes in the PW between 2003 and 2019: Salinity stratification increased as the salinity difference between 155 and 55 m increased by 0.63 psu, the PW layer became thinner by 40–50 m and the Polar-Atlantic front moved ∼10 km west in June 2015. All processes point to an "Atlantification" of the western Fram Strait and a reduced Polar outflow. Including the novel data sets reduced the uncertainty of the FWT to an average of 8% after 2015, as opposed to 17% in earlier estimates.

Plain Language Summary

The East Greenland Current (EGC) brings fresh and cold Polar Water (PW) southwards from the central Arctic Ocean. In the Fram Strait, between Greenland and Svalbard, the strength and properties of this current have been observed using moored instruments since 1997. We present updated time series for the 2015–2019 period and re-analyze earlier variability and estimates. Our results indicate that the fresh water transport since 2015 has decreased, however, with an exception in 2017. This general decrease is caused by a reduction in the southward flow speed and the amount of fresh Polar Water. The front between Polar and Atlantic water has moved westward, and the Polar Water layer has become thinner and more stratified. Moreover, the amount of Atlantic Water in the section increased, pointing to an "Atlantification" of the western Fram Strait. We also refine the time series of the EGC back in time based on the new data, calculate the uncertainty, and show how it depends on the amount of instruments. Finally, we evaluate possible drivers of the observed changes and discuss a connection with Arctic freshwater storage.

1. Introduction

The Arctic is experiencing rapid changes related to anthropogenic climate change (Haine, 2020; Jahn & Laiho, 2020). Arctic warming and rising air-temperature lead to a more intense hydrological cycle and rapid ice retreat, leading to increased liquid freshwater input to the Arctic Ocean (Collins et al., 2013; Graham et al., 2017; Shu et al., 2018). Freshwater (both liquid and sea-ice) circulate in the central Arctic Ocean with the surface currents and exit through the Fram Strait and the Canadian Arctic Archipelago (Figure 1). Freshwater anomalies entering the Nordic Seas and Subpolar North Atlantic may modify dense water formation and therefore the strength of the Atlantic Meridional Overturning Circulation (AMOC) (Heuzé, 2017; Le Bras et al., 2021; Stommel, 1961). So far, however, measurements of the AMOC reveal strong variability and the current length of the time series has been shown to be too short in order to identify a significant trend (Lobelle et al., 2020). Motivated by the observed rapid increase of the fresh water storage in the Arctic in the 2000s (McPhee et al., 2009; Proshutinsky et al., 2009, 2019; Rabe et al., 2014), and the projected freshening by the end of the century (Collins et al., 2013; Jahn & Laiho, 2020; Lique et al., 2016; Shu et al., 2018), we analyze the Arctic freshwater outflow through the Fram Strait, as it reflects changes occurring in the central Arctic Ocean and precedes variability in the Nordic Seas and the Subpolar North Atlantic.

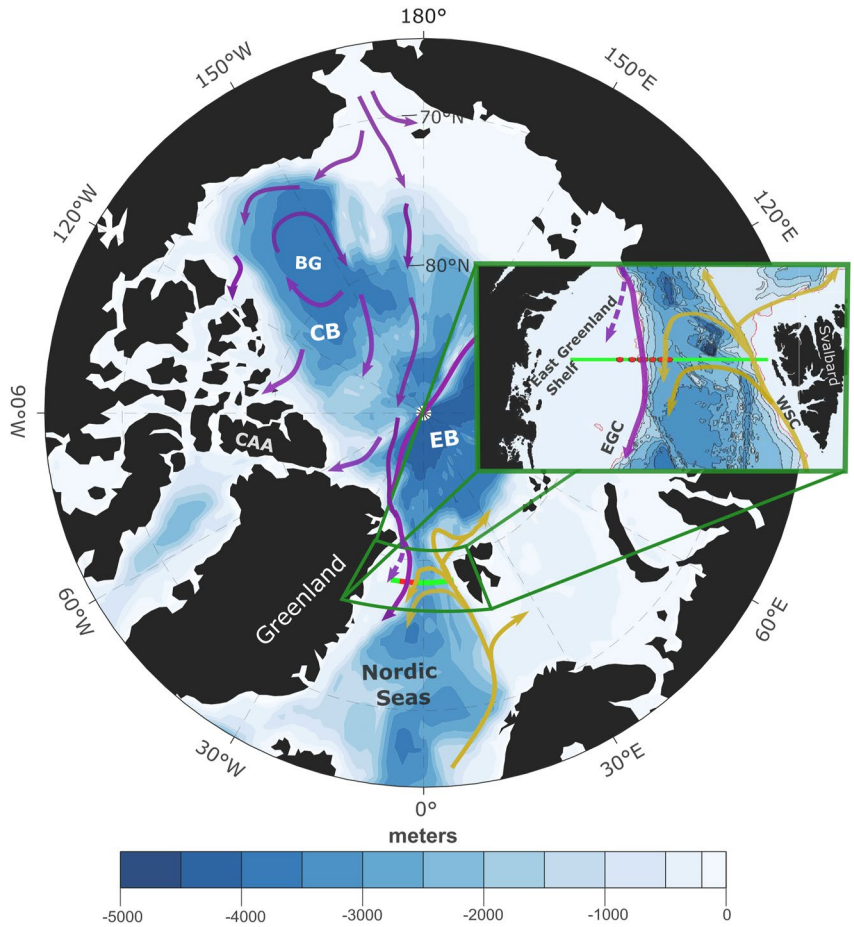

Figure 1. Map of the central Arctic Ocean and Nordic Seas with focus on the Fram Strait. Across the strait, the red dots indicate the mooring array of the Fram Strait Outflow Observatory, and the green line the annually repeated CTD section. The yellow arrows indicate the pathways of Atlantic Water into the Arctic and the West Spitsbergen Current. The purple arrows indicate the suggested pathways of freshwater in the central Arctic Ocean and the East Greenland Current (Rudels, 2009). The purple dashed arrow over the Greenland shelf suggests the pathway of Polar Waters transported over the shelf and not captured by the mooring array. The initials: EB, CB, BG, and CAA stand for the: Eurasian Basin, Canadian Basin, Beaufort Gyre and Canadian Arctic Archipelago, respectively.

The Fram Strait lies between Northeast Greenland and the Svalbard archipelago (Figure 1) and is the largest and deepest gateway between the central Arctic Ocean and the Nordic Seas. The deep part of the strait has a maximum depth of around 2600 m and steep slopes connect it to the much shallower continental shelves of Greenland and Svalbard. Following the continental slope on the western side of the strait, cold and fresh Polar Water (PW) and sea-ice are exported from the Arctic with the East Greenland Current (EGC) (Aagaard & Carmack, 1968). Along the continental slope to the east, the West Spitsbergen Current (WSC) brings warm Atlantic Water (AW) to the central Arctic Ocean (Mosby, 1962), while branches of AW recirculate within the Fram Strait and flow southward alongside the PW (Quadfasel et al., 1987). The EGC carries about half of the liquid freshwater export of the Arctic Ocean and nearly 90% of the sea-ice (see Haine et al. (2015) and references therein). Despite the challenging field conditions in the western Fram Strait, a large and up-to-date data set has emerged from the ocean moorings of the Fram Strait Arctic Outflow Observatory (FSAOO), providing hydrographic and current data from the EGC, over and near the continental slope, at 78°50'N since 2002 (79°N before that). The moorings of the FSAOO allow the study of the year-round Arctic freshwater outflow occurring through the mooring array (De Steur et al., 2018), however, the east Greenland shelf remains undersampled and the fresh water transport over the shelf is poorly known, remaining the largest unknown in the southward freshwater outflow to southern latitudes (Foukal et al., 2020).

Freshwater content in the ocean is defined as the amount of zero-salinity water required to reach an observed salinity, starting from a chosen reference value (Haine et al., 2015). One of the first indications of an increasing freshwater content in the Arctic Ocean came by Proshutinsky et al. (2009), who reported an increase of the fresh water content in the Beaufort Gyre between 2003 and 2007. Rabe et al. (2014), using both observations and model data reported a rapid Arctic-wide increase of the fresh water content between 2000 and 2009. This increase was accompanied by an intensification of the Beaufort Gyre leading to convergence of freshwater in the area (Giles et al., 2012; Proshutinsky et al., 2009; Rabe et al., 2014) and possibly to a reduction of the Arctic freshwater outflow. In accordance with that, De Steur et al. (2009) identified a decrease in freshwater outflow through the Fram Strait between 2005 and 2009, while other studies reported no significant changes (Marnela et al., 2016; Rabe et al., 2013). Between 2009 and 2015 the spin-up of the Beaufort Gyre and the freshening of the Canadian Basin equilibrated (Zhang et al., 2016), but since 2016 the freshening continued (Proshutinsky et al., 2019). The last record of the observed liquid freshwater outflow through Fram Strait showed a period of increased fresh water transport between 2010 and 2015, concurrent with the equilibration of the Beaufort Gyre, and accumulation to a significant freshwater volume anomaly (De Steur et al., 2018). After 2015, it is unclear if the fresh water transport in the Fram Strait continued to increase, or if it has decreased, possibly in response to an intensifying Beaufort Gyre. However, new mooring data have become available since then, and these are incorporated here.

In this paper, we present updated fresh water transport estimates through the western Fram Strait based on year-round ocean mooring records collected by the FSAOO between 2015 and 2019. Moreover, we correct estimates from the previous years, which had fewer instruments, to make a consistent time series allowing for comparison. We show that the large increase in fresh water transport observed by De Steur et al. (2018) did not continue after 2015, however, interannual variability has been large. We present the total volume transport and freshwater content through the full depth mooring array as well as for the Polar Water only, and describe changes in hydrography and current properties between 2003 and 2019. To address concerns related to the dependence of fresh water transport on a reference salinity (Schauer & Losch, 2019), we additionally provide salt transport values, as salt transport is independent of a reference value, and discuss the strengths and limitations of the two variables. Finally, we calculate the uncertainty of fresh water transport and show how this has decreased over time with increasing instrument coverage.

2. Data and Methods

2.1. Mooring Data

Since 1997 and up to the present, high-frequency year-round hydrographic data have been collected by the moorings of the FSAOO maintained by the Norwegian Polar Institute. The moorings are positioned across the East Greenland Current, between 0.3°W and 8°W longitude (Figure 1) (De Steur et al., 2014). Between September 2015 and August 2016, the year of maximum instrument coverage, the array consisted of eight moorings: F9, F10, F11, F12, F13, F13b, F14, and F17 positioned at: 0.75°W, 2°W, 3°W, 4°W, 5°W, 5.5°W, 6.5°W, and 8°W longitude, respectively (Figure 2b). Moorings F9 and F10 have been operated by the Alfred Wegener Institute until September 2016. Since then, F9 has been discontinued and since 2017, the Norwegian Polar Institute has continued F10. The configuration of FSAOO has changed significantly over the years (Figure 2c). This is because more moorings, instruments and technologies have been implemented, increasing the spatial coverage of the array. In addition, however, there have been periods with significant data gaps due to lost moorings, for example, between September 2004 and August 2005, the year with the most data gaps (Figure 2a) (De Steur et al., 2014, 2018).

A prominent improvement in the composition of FSAOO took place in September 2003 when mooring F17 was added at 8°W resulting in a better coverage of the southward fresh water transport (FWT) (De Steur et al., 2018). As of September 2015, mooring F13b was added over the continental slope. Overall, the number of sampling points of the FSAOO has increased significantly in recent years providing better coverage of the EGC (Figure 2c). This study focuses on the moorings F10 through F17 between September 2003 and September 2019. Mooring F9, which has not been operated since September 2016, is excluded from this analysis.

In general, the array contains a combination of Seabird sensors (SBE 16, 37) measuring in situ conductivity, temperature and pressure, of Recording Current Meters (RCM 7, 8, 9, 11) measuring horizontal velocities, temperature and depth, and of Aanderaa Doppler Current Meter (DCM12), Aanderaa Recording Doppler Current

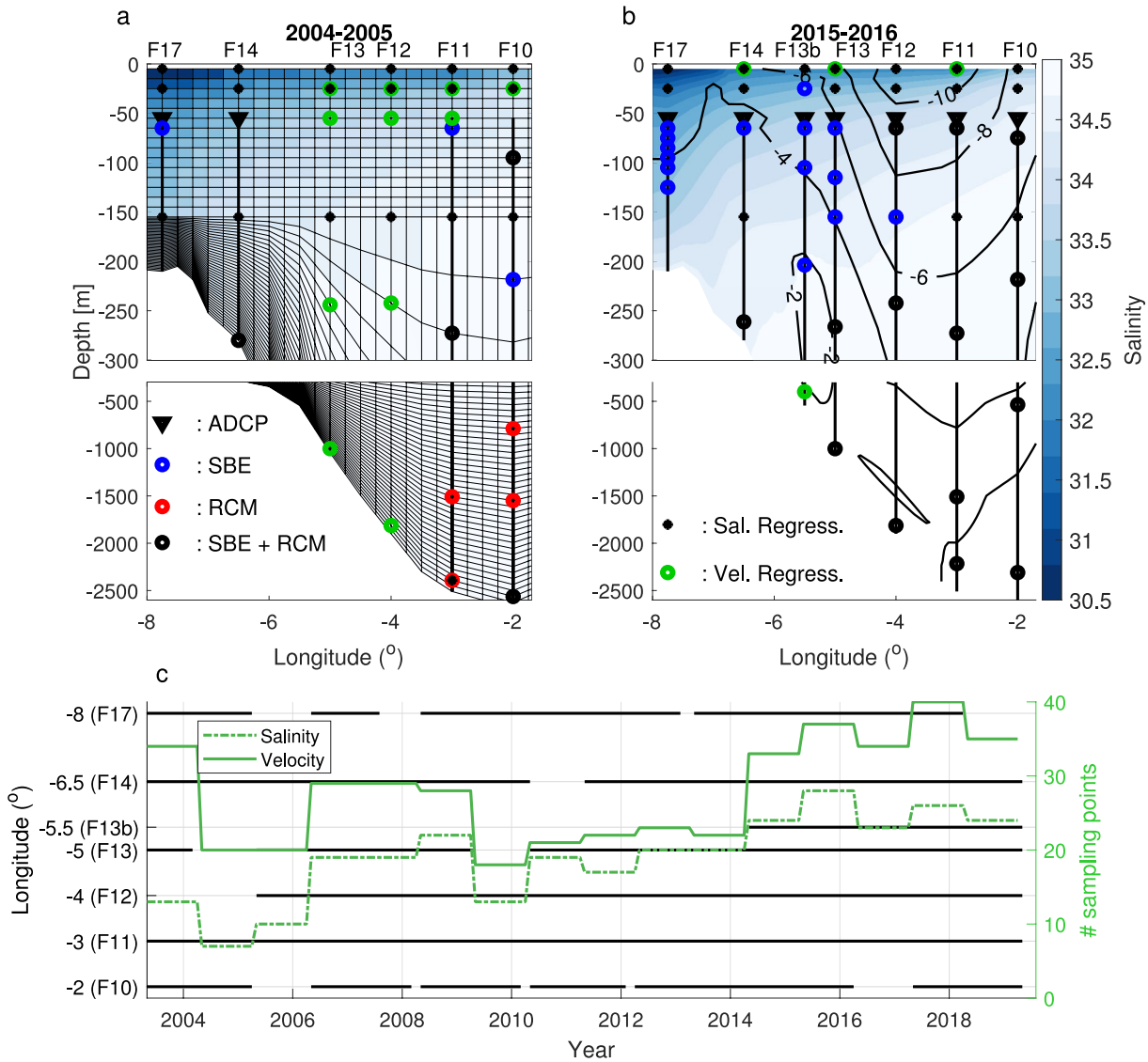

Figure 2. (a and b) Setup of instruments in the Fram Strait Outflow Observatory (FSAOO) between Sept. 2004–Aug. 2005 and Sept. 2015–Aug. 2016. The color shading and the black contours (b) show the 2003–2009 mean salinity and velocity from the moorings, and the mesh (a) shows the interpolation grid. The colored dots show the interpolant positions. The big black dots show positions of combined velocity (RCM) and salinity-temperature sensors, the blue and red dots positions of salinity-temperature or velocity sensors only and the black triangles upward-looking acoustic Doppler velocity profilers. The green dots show the positions of velocity regression, and the small black dots the positions of salinity regression. (c) Sampling-point number of the FSAOO for salinity and velocity per year-deployment (right axis). The horizontal black lines indicate the deployment period for each mooring (left axis).

Meter (RDCP600), or RDI Acoustic Doppler Current Profilers (ADCP) installed at ~55 m providing velocity profiles between 50 and 10 m below the surface. The sampling intervals of salinity, velocity, temperature and pressure vary between 15 min and 2 hr (De Steur et al., 2014).

Since most of the FWT occurs in the upper water column, near-surface salinity and velocity measurements are essential. However, the acquisition of year-round salinity data in the top 50 m of the water column has been challenging due to the presence of icebergs and deep-reaching sea-ice keels that, in early years, did not allow the deployment of instruments near the surface. Between 2013 and 2019, four Inductive Modem (IM) SBE37 Microcats (so-called IceCATs) were deployed with a weak link (Curry et al., 2014) at 25 m target depth (F13b: 2015, 2017, F17: 2013, 2014), providing year-round data of near-surface salinity for the first time. Another significant addition to the instrumentation of FSAOO was the deployment of extra SBE37 sensors between 70 and 170 m

depth, at moorings F12 to F14 (F12: 2016, 2018, F13: 2013–2018, F13b: 2014–2018, F14: 2016, 2018), which reduced interpolation errors between instruments at ∼55 and 250 m depth.

2.2. Additional Data

Since the first deployment of the mooring array, a CTD section is repeated every August/September during the annual maintenance of the array. In addition, five CTD sections from cruises crossing the Fram Strait during April/May are available (2002, 2005, 2007, 2008, and 2018). The CTD sections provide high-resolution data (1m in the vertical, and 5–10 km in the horizontal) of in situ salinity and temperature, which are interpolated on the same grid as the moorings (Section 2.3). A monthly time series of salinity based on the CTD data set is used to complement the mooring data set by, (a) providing an estimate of the undersampled near-surface salinity in the absence of IceCATs and (b) improving interpolation bias in the absence of instruments at ∼155 m. This CTD time series consists of the year-specific September and May data, which are interpolated cubically to provide a first-order estimate of the seasonal cycle for each year. For years with no May observations, the long-term mean May value is used. Finally, we use the September CTD data before gridding to calculate the geostrophic velocity from the equation of thermal wind balance, referenced to zero velocity at the bottom.

Additional monthly mean 10 m meridional-wind data (0.25° resolution) taken from European Center for Medium-Range Weather Forecasts Reanalysis v5 (Hersbach et al., 2020) are used to examine the relation between EGC volume transport and wind velocity over the Fram Strait.

2.3. Gridding of Data

For the calculation of transport through the array, we interpolate the monthly averaged velocity and salinity data from the moorings on a grid with 0.25° horizontal resolution (∼5.3 km). Moreover, to represent properties over the steep continental slope, we use a bottom following grid below 155 m, and thus vertical resolution varies in space (Figure 2a) (De Steur et al., 2014). However, in case of data gaps due to the lack or loss of instrumentation, and to limit interpolation bias and avoid extrapolation, estimations of monthly averaged salinity and velocity need to be added at essential positions in the cross-section. For velocity, this is done with linear regression from nearby instruments, with coefficients from other years' deployments, while salinity gaps are filled with linear regression from nearby instruments, with coefficients from the CTD time series. The remaining gaps are filled with the long-term mean for both variables (see Text S1 in the Supporting Information S1). Then, the monthly averaged velocity is linearly interpolated on the grid, and mooring salinity is cubically interpolated in the vertical and linearly interpolated in the horizontal. Finally, the gridded salinity data are combined with temperature data (that followed the same process) to obtain density, and salinity is checked against and corrected for any density inversions.

2.4. Methods

As of September 2013, the novel instruments provide year-round observations of salinity at 25 m (IceCATs) and 155 m (SBE37), improving our understanding of near-surface salinity seasonality and stratification. Since September 2014, the newly deployed mooring F13b provides data at 5.5°W, near the western edge of the core of the EGC. However, it is unclear how the previous transport estimates, when those instruments were not deployed, compare to those from recent years. To account for that, we exclude those three datasets, and in their absence calculate the offset of salinity and/or velocity. Then, we correct the previous estimates for the calculated offsets and recalculate the FWT (Section 3.1).

We address the spatial and temporal variability of the EGC by comparing the mean gridded salinity and velocity fields for three averaging periods: period 1 between Sept. 2003 and Aug. 2009 showing relatively stable FWT from the EGC (De Steur et al., 2009); period 2 between Sept. 2009 and Aug. 2015 showing occurrences of increased FWT (De Steur et al., 2018) and period 3, after Aug. 2015, for which we present the updates of FWT. To make sure that the observed changes do not relate to the changing array configuration we use the corrected time series of salinity and velocity. We examine the changes in salinity stratification with the salinity difference between 55 and 155 m, as well as the changes in the extent of the Polar Water across the EGC (Section 3.2).

Polar Water (PW) is defined as the water with negative temperature ($T < 0$°C) and potential density anomaly (σ_θ, referenced at the surface) less than 27.7 kg/m^3 (Rudels et al., 2005).

The fresh water and salt transport are determined as:

$$FWT_{(t)} = \int_{L_0}^{L_1} \int_{Z_0}^{Z_1} V_{(t,x,z)} \frac{S_r - S_{(t,x,z)}}{S_r} dzdx, \quad (1)$$

$$ST_{(t)} = \int_{L_0}^{L_1} \int_{Z_0}^{Z_1} V_{(t,x,z)} S_{(t,x,z)} \rho_{(t,x,z)} dzdx, \quad (2)$$

while the volume transport and freshwater content are:

$$VT_{(t)} = \int_{L_0}^{L_1} \int_{Z_0}^{Z_1} V_{(t,x,z)} dzdx, \quad (3)$$

$$FWC_{(t)} = \int_{L_0}^{L_1} \int_{Z_0}^{Z_1} \frac{S_r - S_{(t,x,z)}}{S_r} dzdx, \quad (4)$$

with $V_{(t,x,z)}$ and $S_{(t,x,z)}$ the velocity and salinity, and $\rho_{(t,x,z)}$ the density calculated from salinity and temperature. We set the reference salinity S_r to 34.9, the mean salinity of the Nordic Seas (Holfort & Meincke, 2005), but FWT is provided between brackets as well for $S_r = 34.8$, the mean salinity of the central Arctic Ocean (Aagaard & Carmack, 1989). In the horizontal, we integrate between F10 ($L_o = 2$°W) and F17 ($L_1 = 8$°W) while in the vertical we distinguish two cases: (a) Integration across the full vertical section ($Z_0 = 0$, $Z_1 = Z_{\text{bottom}}$), and (b) integration across the PW ($Z_o = 0$, $Z_1 = Z|_{\text{PWdepth}}$) (Section 3.3).

The uncertainty in the calculation of FWT originates from the limited spatial coverage of the mooring array. More specifically, there are two types of uncertainty: The uncertainty of the interpolants and the uncertainty of gridding. The first refers to the uncertainty of the estimated values of velocity and salinity before gridding. This includes the sampling uncertainty of the instruments, the regression uncertainty from nearby instruments, and the uncertainty of gap-filling with the long-term mean (see Text S1 in the Supporting Information S1). The second refers to the uncertainty of interpolating between a limited number of interpolants (Figures 2a and 2b), thus lacking details of the spatial variability. To estimate the uncertainty of gridding we use the mean section of the September CTD-dataset as the baseline, we sub-sample the salinity and geostrophic velocity (see Section 2.2) sections at the interpolant positions, re-grid, and calculate the approximated FWT. Then, we use the absolute difference from the FWT of the baseline as the uncertainty. To include the uncertainty of the interpolants we allow random deviations from the baseline values, with the maximum deviation depending on the interpolant category and of its position in the section (see Text S1 in the Supporting Information S1), then calculate five hundred ensembles of the approximated FWT, and define the root-mean-square difference from the baseline value as the uncertainty (Section 3.4).

3. Results

3.1. Novel Data

The CTD time series provides a first estimate of the seasonal cycle of salinity. Resulting from cubic interpolation between monthly averages from early September and May, it disregards any variability on shorter time scales. The salinity difference between 25 and 55 m observed by the year-round IceCAT deployments (ΔS_{obs}) shows some clear differences from the one estimated by the CTD time series (ΔS_{ctd}), as it experiences abrupt changes within short periods (Figure 3). More specifically, during short periods in late September, early October, that is, after the annually repeated CTD section, ΔS_{obs} increases as much as 1.3 psu/day reaching the maximum stratification in October, which is not resolved by ΔS_{ctd}. In the core of the EGC at mooring F13b (Figures 3d and 3h), ΔS_{obs} experiences a sharp decrease in November–December, and remains well mixed up to late February–early March. On the shelf at mooring F17 (Figures 3c and 3g), ΔS_{obs} indicates well-mixed conditions in November and February in both deployments, while December and January differ between the two deployment years.

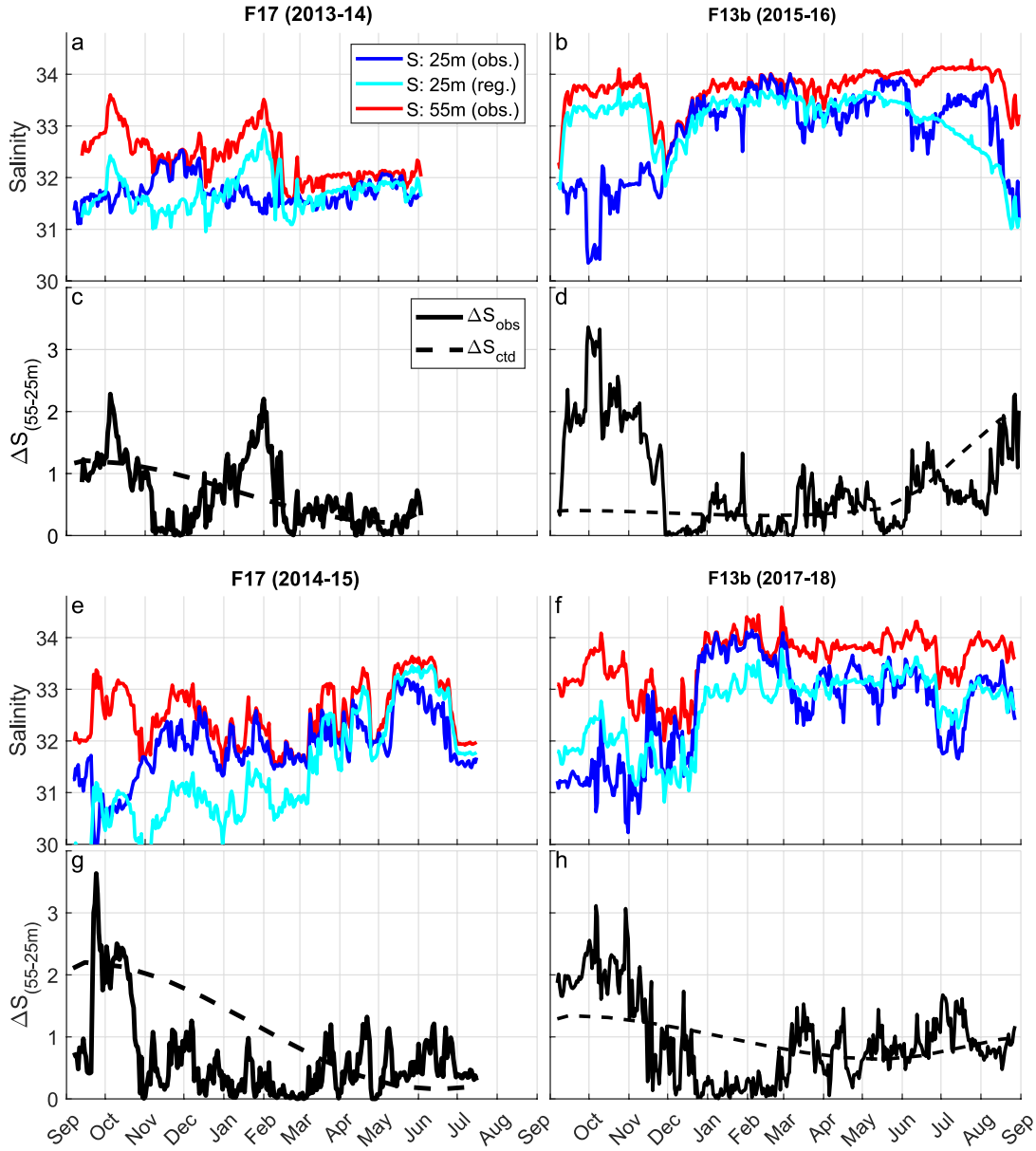

Figure 3. (a,b,e, and f) Observed (obs.) and regressed (reg.) daily means of salinity at 25 m from the four IceCAT deployments, and salinity at 55 m from the same mooring and year. (c,d,g, and h) Observed salinity difference between 25 and 55 m (ΔS_{obs}) and the one calculated from the CTD time series (ΔS_{CTD}).

The year-round near-surface salinity of the EGC in the Fram Strait shows prominent seasonal variability (Figure 3). The salinity at 25m decreases in August–September due to freshwater input from ice-melting, while between November and March a strong mixed layer is formed due to the loss of summer stratification, mixing, and brine rejection (Figures 3b, 3e, and 3f). Those patterns are partially local processes (e.g., melting ice, brine rejection, mixing), and partially advected, in particular when the freshening continues until well into November. Another consistent seasonal pattern is a salinity maximum at 55 m observed between September and November (Figures 3a, 3b, 3e, and 3f). These high values are likely not attributed to local processes, and could be advected from the Arctic. However, these four records show there is substantial monthly and interannual variability, illustrating the need for consistent monitoring of near-surface salinity.

The differences between ΔS_{obs} and ΔS_{ctd} result in an offset between the observed (IceCATs) and regressed salinity at 25 m (Figures 3a, 3b, 3e, and 3f), and thus between the respective fresh water transports (FWT). Similarly, we

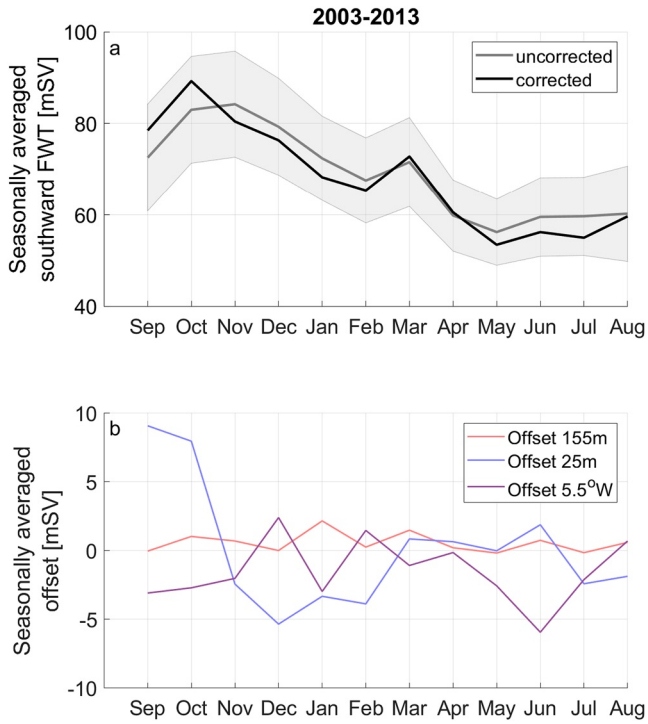

Figure 4. (a) Southward fresh water transports (FWT) seasonally averaged between 2003 and 2013, before and after the correction based on the novel data. The envelope shows the seasonally averaged uncertainty of FWT for the same period. (b) Contributions of the three different novel datasets (IceCATs at 25 m, SBE37 at 155 m, mooring F13b at 5.5°W) to the total offset.

calculate the offset related to the newly introduced mooring F13b at 5.5°W (Sept. 2014), and with the SBE37 sensors deployed at ∼155 m (After Sept. 2013). Then, in the absence of these novel data, we correct the time series for those offsets. The correction of the time series is described in more detail in Text S2 in the Supporting Information S1.

Seasonally averaged between Sept. 2003–Sept. 2013, prior to the deployment of these new instruments, the correction results in a small decrease of the mean FWT by 0.8 mSV (Figure 4a), as the different offsets (varying from −6 mSV to +9 mSV) compensate each other (Figure 4b). More specifically, the SBE37 sensors introduced at 155 m result in a mean increase of 0.5 mSV by better resolving salinity in the lower halocline, and the mooring F13b at 5.5°W contributes to a mean decrease of −1.5 mSV by limiting interpolation errors at the western boundary of the EGC in summer and autumn (Figure 4b). Finally, the mean offset from the IceCATs deployed at 25 m, and the corrections based on these data (see Text S2 in the Supporting Information S1) are small, however, with significant seasonal variation. The September and October FWT increases (9 mSV), reflecting the high stratification and low salinity observed at F13b (Figures 3b and 3f), but decreases between November and February (4 mSV), reflecting the well-mixed and more saline conditions in winter. Overall, the corrected time series remain within the uncertainty limits (Section 3.4) of the earlier estimates, implying that the time series of FWT in the EGC is not impacted significantly by the changing composition of the FSAOO array.

3.2. Hydrography and Current Velocity

Here, to allow comparison with earlier years, we present the corrected salinity and velocity data and analyze them for the three periods defined in Section 2 (period 1: Sept. 2003–Aug. 2009, period 2: Sept. 2009–Aug. 2015, period 3: Sept. 2015–Aug. 2019). A test case where the novel instruments were excluded was tested and showed similar results. The mooring domain extends across the continental slope of Greenland between 8°W and 2°W, covering the deep western Fram Strait and a part of the shelf (8°W-6°W). Close to the surface, two water masses are present. To the west, the southward moving buoyant Polar Waters (PW) with $T < 0$°C and potential density anomaly (σ_θ) smaller than 27.7 kg/m^3, and to the east and beneath the PW, the denser recirculating Atlantic Water (AW) (Figure 5a). The properties and position of the two water masses result in a tilt of the isopycnals and in a surface-intensified southward flow. Those two water masses form the EGC with its core between 5°W and 2°W (Figure 5d).

Figures 5b and 5c show the salinity anomaly (ΔS) in periods 2 and 3 relative to period 1. In period 2 the fresh near-surface water (σ_θ <= 26.5 kg/m^3) became fresher (Figure 5b), while the layer below experienced only small changes. In period 3, the top layer remains fresher than in period 1 (Figure 5c), but the denser PW of the lower halocline experiences a significant increase in salinity. The freshening in the upper ocean is maximum in November–December, followed by September–October, and is minimum in May–July where it is limited to the shelf. Salinification below the 26.5 kg/m^3 isopycnal occurs during all months and does not show a seasonal pattern (results not shown). This salinification is accompanied by an increase in temperature of the denser PW shown by the upward and westward shift of the $T = 0$°C isotherm, which here defines the limit between PW and AW (Figure 5c). This shrinking of the PW domain is associated with an increased presence of AW in the section. The data do not support an intensified recirculation of AW at this latitude, as the zonal component of the velocity shows a weaker westward flow during period 3 (Figure 6b), however, increased recirculation of AW could have occurred upstream of our array.

Figures 5d and 5f show the meridional velocity averaged over the three periods, and the anomaly of the two latter periods relative to period 1 is shown with contours (Figures 5e and 5f). In period 2, an additional shallow surface intensified current core is observed over the shelf. This shelf current transports fresh PW southwards and likely

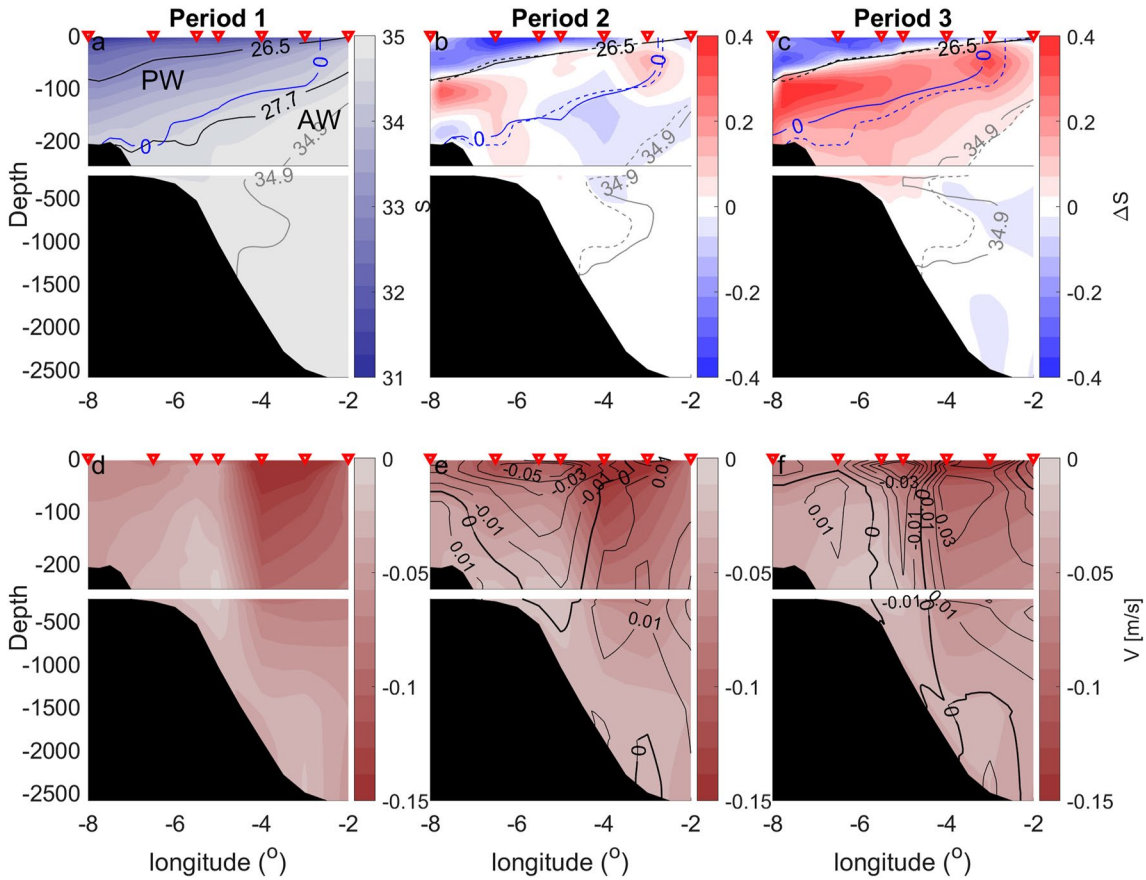

Figure 5. (a) Mean salinity section over period 1, (b and c) salinity anomaly of periods 2 and 3 relative to period 1. The solid contours indicate the mean position of the isopycnals $\sigma_\theta = 26.5$ kg/m^3, and $\sigma_\theta = 27.7$ kg/m^3 (black), the isotherm $T = 0$°C (blue) and the isohaline $S = 34.9$ psu (gray) in each period. The dashed contours in b and c indicate the mean position of the isolines over period 1. (d and f) Mean velocity section over the three periods. For period 2 and 3 the contours show the anomaly relative to period 1.

represents a part of the Polar Surface Water Jet described by Håvik et al. (2017). This current contributes to the increased FWT observed in period 2. In period 3, the shelf current weakens, and only a narrow belt over the slope (centered at 5°W) on the western limit of the EGC maintains higher velocity compared to period 1, while the deeper core of the EGC east of 4°W weakens significantly. Overall, in period 3 the EGC appears to be weaker than in period 1 and 2, but wider than period 1.

Southward velocity averaged over the top 155 m increased from 8 cm/s in period 1–9 cm/s in period 2, while in period 3 it decreased to 7 cm/s, though showing increased seasonality (Figure 6a). Similarly, salinity increases in period 3, as the salinification of the lower halocline exceeds the freshening observed in the top layer (Figure 6c). This salinification in the halocline results in shallower isopycnal depth (e.i. $\sigma_\theta = 27.7$ kg/m^3). This is less prominent at the eastern part of the domain (4°W to 2°W) (Figure 6d), resulting in a relaxation of the isopycnal tilt. This suggests that the observed weakening of the EGC is related partly to a decrease of the zonal gradient of density. From the September CTD data we calculate the geostrophic velocity, referenced to zero at the bottom (Figure 6a) (we exclude September 2014 which deviated more than three standard deviations from the mean), and find it to account for 51% of the observed (mooring) velocity in September months, while 67% of the observed velocity decrease between periods 2 and 3 is explained by the reduction of the geostrophic velocity (seen in the CTD sections).

The changes in the spatial distribution of salinity in the western Fram Strait show increasing stratification in the PW, and a decreased depth and eastward extent of the PW domain related to increased presence of AW. Firstly, we present the changing salinity stratification of the PW with the mean salinity difference between 55 and 155 m

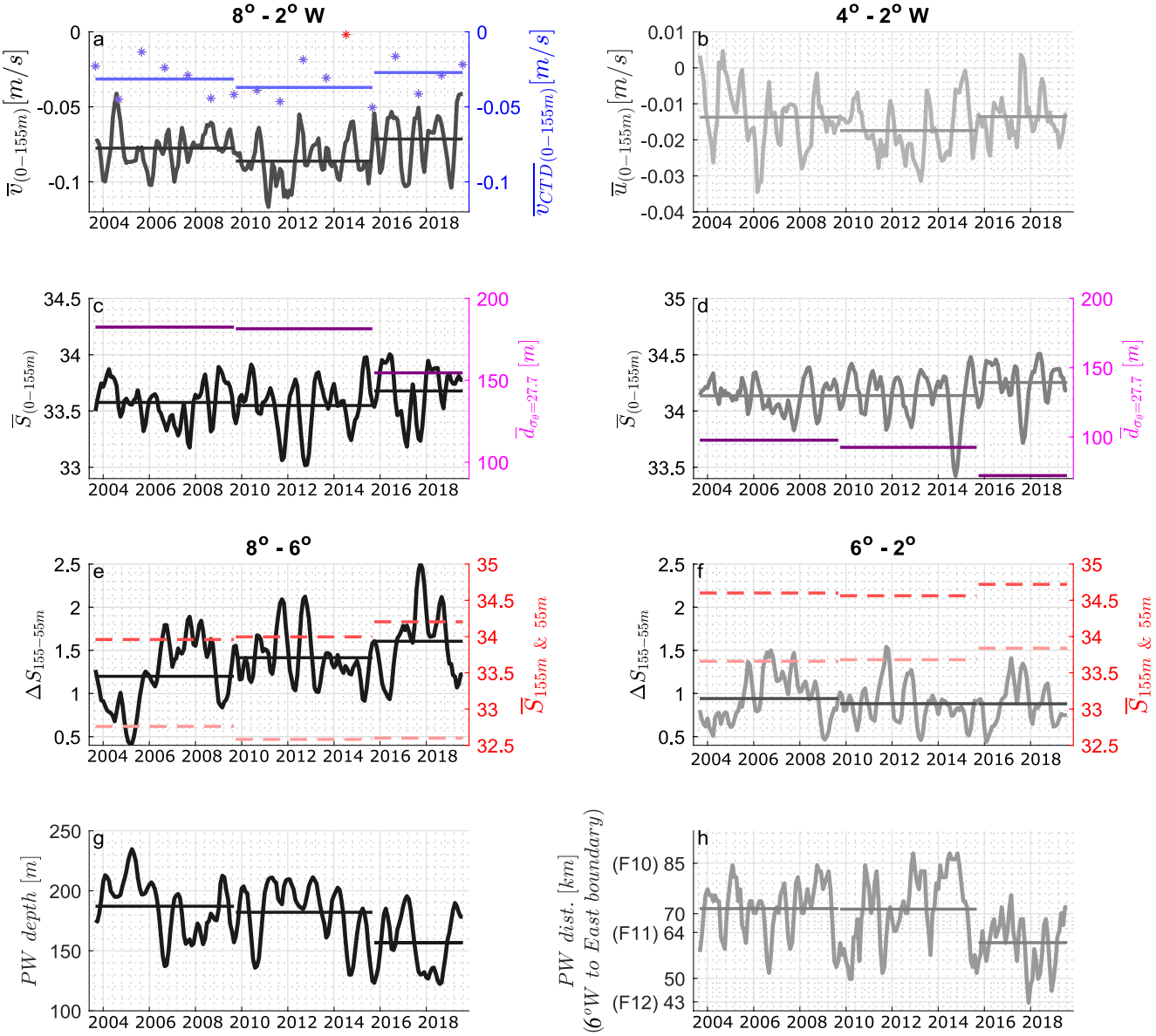

Figure 6. (a and b) Mean meridional velocity between 8° and 2°W, and zonal velocity between 4°W-2°W averaged in the top 155 m. The meridional geostrophic velocity (referenced to zero at the bottom calculated from the Sept. CTD data) is presented with the blue stars (the red star shows the anomalous month of Sept. 2014 which is excluded from the calculations). (c and d) Mean salinity between 8°W-2°W, and between 4°W-2°W averaged in the top 155 m. The average depth of the $\sigma_\theta = 27.7$ kg/m^3 isopycnal is presented for the three periods with the magenta lines. (e and f) Salinity difference between 55 and 155 m depth, averaged between 8°W-6°W and 6°-2°W. The mean values of salinity at 55 and 155 m are shown with the red (155 m) and pale red (55 m) dashed lines. (g) Polar Water depth defined as the lower limit of the Polar Water averaged between 8°W-6°W, and (h) Polar Water distance defined as the surface distance of the PW-AW front (0°C isotherm) from 6°W.

(ΔS_{55-155}), averaged over the shelf from 8°W to 6°W (Figure 6e). Between periods 1 and 2, ΔS_{55-155} increased from 1.2 to 1.4 psu, following the freshening at 55 m depth, and in period 3 it continued increasing reaching 1.6 psu, this time due to the salinification at 155 m. We note the difference of the shelf with the eastern part of the domain, where salinity stratification does not change significantly (Figure 6f), as salinity is increasing both at 55 and 155 m due to higher presence of AW over the whole depth. Finally, we quantify the retreat of the PW layer with the PW depth (Figure 6g), defined as the lower limit of the Polar Water averaged between 8°W and 6°W, and the PW distance (Figure 6h), indicating the distance of the PW-AW front (i.e., the 0°C isotherm) at the surface from 6°W. Both these variables experience a significant decrease in period 3: PW depth decreases from 182 m in period 2–157 m in period 3, while PW distance retreats from 71 km east of 6°W in period 2–61 km in period 3.

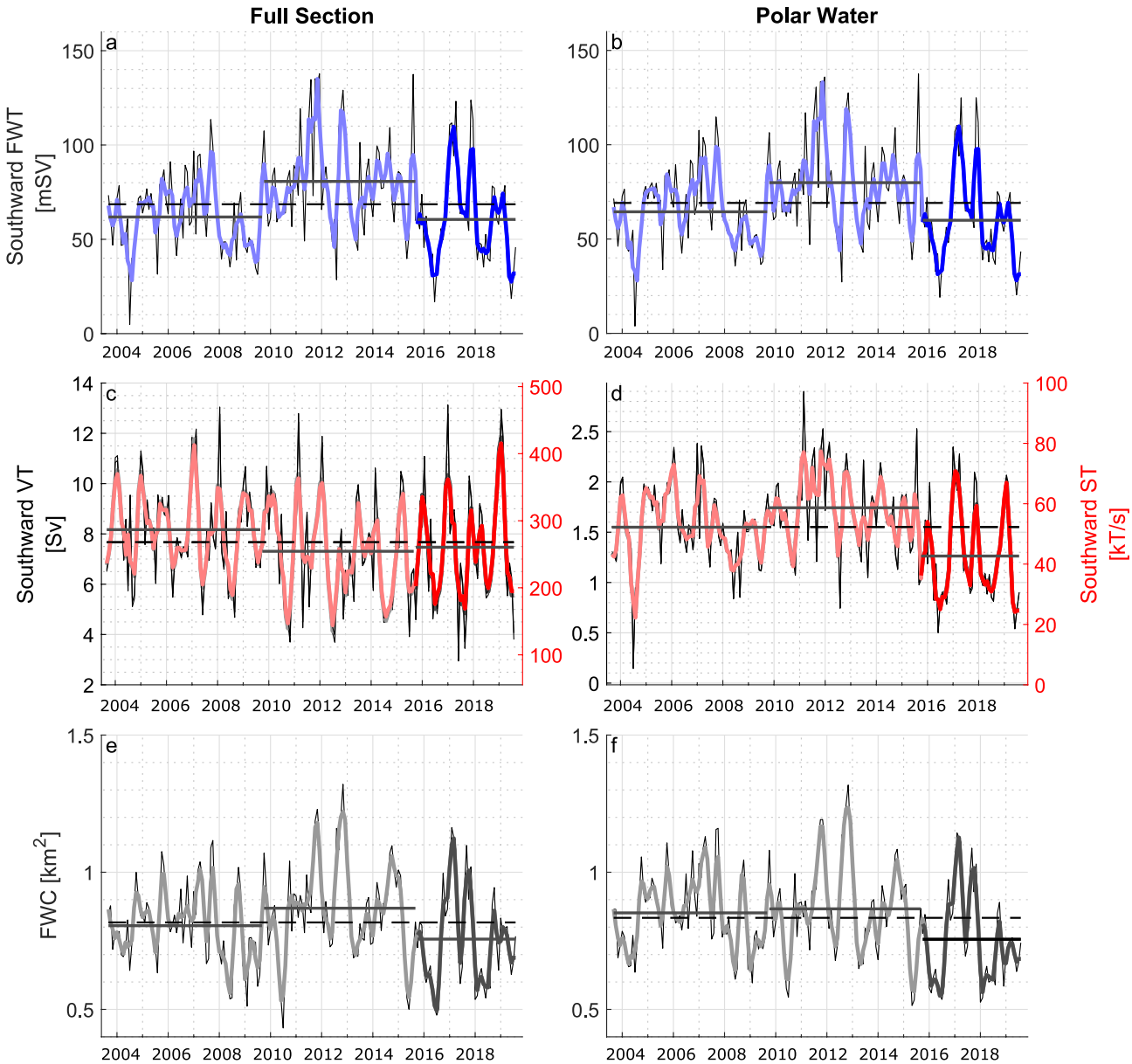

Figure 7. Time series of southward freshwater (a and b), salt and volume transport (c and d), and freshwater content (e and f) integrated in the full vertical section (left), and the Polar Water ($\sigma < 27.7$ kg/m^3, $T < 0$°C) (right) ($S_{ref} = 34.9$). The thin-black and thick-colored time series indicate the monthly values and 3-month running means, respectively. The horizontal lines indicate the long-term means (dashed: Sept. 2003–Aug. 2019) and the means over the three averaging periods (solid: period 1: Sept. 2003–Aug. 2009, period 2: Sept. 2009–Aug. 2015, period 3: Sept. 2015–Aug. 2019).

3.3. Transport of Freshwater and Salt

Here, we present the monthly mean time series of transport (Figure 7) for the two areas of integration, that is, (a) the full vertical section and (b) PW only, both corrected for the introduction of novel instruments. Due to the southward flow of the EGC, the transport from the current is defined as positive to the south. Along with the fresh water transport (FWT) (Figures 7a and 7b) and salt transport (ST) (Figures 7c and 7d, red line), we show the volume transport (VT) (Figures 7c and 7d, gray line) and freshwater content (FWC) (Figures 7e and 7f). FWT and FWC are calculated with respect to reference salinity $S_{ref} = 34.9$ and their values are provided with respect to $S_{ref} = 34.8$ as well between brackets.

The increase of the FWT in the EGC in period 2 (Figures 7a and 7b), identified by De Steur et al. (2018), followed an increase of the VT and FWC in the PW (Figures 7d and 7f), occurring due to the increased-southward velocity

Table 1
The Long-Term Mean Values (Sept. 2003–Aug. 2019) and the Means Over the Three Averaging Periods for the Southward Freshwater, Salt and Volume Transport, and the Fresh Water Content, Integrated in the Full Section and the PW

Domain	Period	Southward Fresh water transp. (mSV)	Southward Salt transp. (kT/s)	Southward Volume transp. (SV)	Freshwater cont.(km^2)
Total	2003–2019	68.6 (46.7)	268.1	7.66	0.81 (0.34)
	1) 2003–2009	61.8 (38.5)	286.7	8.18	0.80 (0.32)
	2) 2009–2015	80.7 (60)	254.4	7.29	0.87 (0.39)
	3) 2015–2019	60.5 (39.3)	260.5	7.44	0.76 (0.28)
Polar	2003–2019	69.1 (64.9)	52.3	1.55	0.83 (0.78)
	1) 2003–2009	64.4 (60.2)	52.2	1.54	0.85 (0.79)
	2) 2009–2015	79.9 (75.1)	58.6	1.74	0.87 (0.8)
	3) 2015–2019	59.9 (56.5)	42.6	1.27	0.76 (0.7)
$S < S_{ref}$	2003–2019	73.15 (66.4)	126.5 (68.3)	3.7 (2)	0.92 (0.81)

Note. The fresh water transport and content are calculated with respect to the reference salinity $S_r = 34.9$ (34.8). The long-term means are given as well for the domain with $S < S_{ref}$, as used in De Steur et al. (2018).

(Figure 6a) and freshening of the top layer (Figure 5b), respectively. In period 3, FWT decreased as a result of lower VT and FWC in the PW, due to the decreased southward velocity of the EGC and the salinification of the lower halocline (Figures 5c and 5f). Hence, the increase in FWT from 2010 to 2014 has not continued, but it has reduced after 2015. We note that in the western Fram Strait, the FWT and FWC are controlled by processes within the PW which accounts for 95% of the FWT and FWC occurring above the isohaline of $S = S_{ref}$. Additionally, we mention that due to their definition, FWC and FWT are larger when integrated up to $S = S_{ref}$, as any salinity higher than the reference results in negative contribution to FWC and FWT (Table 1).

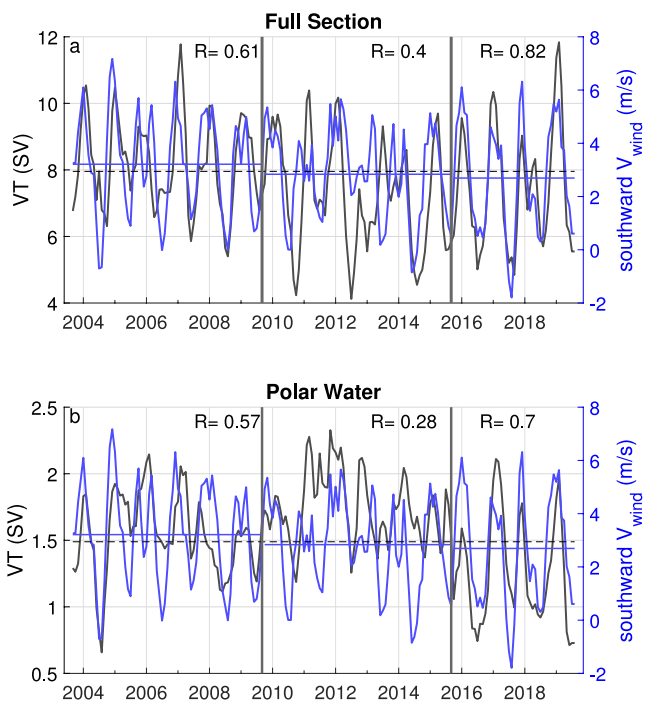

Figure 8. Comparison between southward VT (Figures 7c and 7d) and southward-meridional wind at 10 m over the Fram Strait (ERA5, see Section 2.2). VT is shown for the full section (a) and the Polar Water (b). Wind data are averaged between 8°W-2°W and 78°N-82°N. The correlation coefficient (R) between VT and wind is shown for the three periods.

Focusing on the PW domain (Figure 7), in June 2016 occurred the second lowest FWT event (19.1 (17.7) mSV) since September 2004 (3.8 (3.4) mSV). The low 2016 event was due to a decrease of both the FWC and VT in the PW, while the event in 2004 followed strong southerly winds over the Fram Strait that led to nearly zero transport of PW through the Fram Strait (Figure 8b). Despite a general reduction in FWT in period 3, in 2017 between January–April and November–December, two strong FWT events (125 (119) mSV, 125 (119) mSV) occurred due to the concurring high FWC and VT. The first event happened in concert with a temporal collapse of the Beaufort High and a reversal of surface circulation in the western Arctic (January–March) (Moore et al., 2018), while during the second event, strong northerly winds occurred in the Fram Strait. Finally, in June 2019, a low FWT (20.4 mSV) event followed again a large decrease of the VT partly attributed to a southerly wind anomaly (Figure 8b).

The apparent increased seasonal variability of velocity in period 3 (Figure 6a) contributes to an increase of the FWT variability, as two of the three lowest FWT events of the whole record (June 2016, June 2019) have been observed in period 3, as well as two of the five higher events (January–April, November–December 2017). Moreover, the correlation between the wind velocity and the volume transport over the western Fram Strait increased after 2015 (Figures 8a and 8b). The above are in agreement with a decreasing sea-ice cover in the western Fram Strait (Spreen et al., 2020), and suggests more effective momentum transfer from the atmosphere to the ocean. Overall, since 2015, following the changes in the hydrography and current velocity in

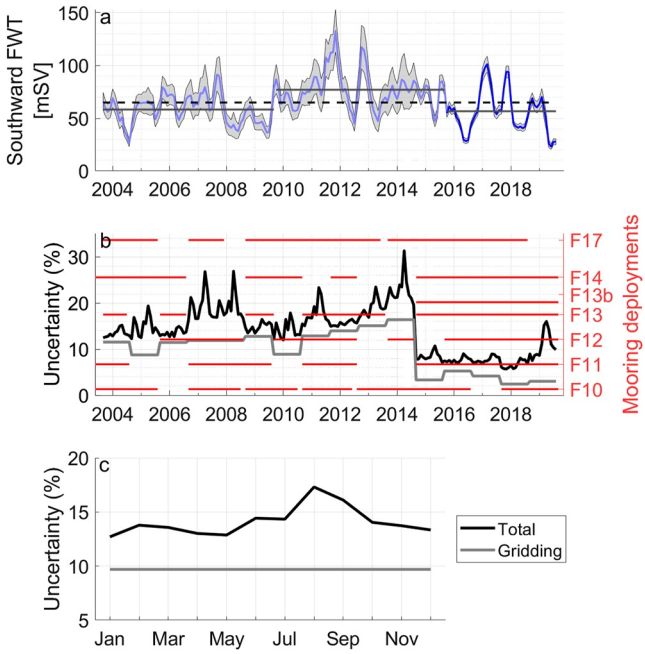

Figure 9. (a) Time series of fresh water transport with the respective uncertainty envelope. (b) Relative uncertainty of the fresh water transport (left axis). The uncertainty of gridding is provided together with the total uncertainty which includes the uncertainty of the interpolants as well. The horizontal lines indicate the mooring deployments with at least one velocity sampling point above 100 m depth (right axis). (c) seasonally averaged uncertainty (2003–2019).

the western Fram Strait, the FWT of the EGC shows a marked change from before, not only in terms of a decrease in the average FWT, but also in terms of increased variability.

A Reynolds decomposition of the FWT through the full depth section (Figure 7a) shows that the velocity anomaly contributes on average 62% (57%), and the FWC anomaly 35% (38%) to the FWT anomaly, while 3% (4%) is the contribution of the cross term anomaly. The ST time series coincides with that of the VT (Figures 7c and 7d), as the velocity anomaly contributes 99.88% to the ST anomaly. For the case of the EGC, and in a fixed boundary domain, the ST variability is defined by velocity only, as the velocity anomaly dominates over the salinity (and density) anomaly. However, in a domain with a (non-fixed) variable boundary, as is the PW layer ($\sigma_\theta < 27.7$ kg/m^3 & $T < 0$°C), part of the variability of VT and ST is explained by the variability of the boundary. Then, the VT and ST in the PW layer (Figure 7d) are a function of velocity and of the area occupied by the PW. Those two contribute 82% (82%) and 18% (18%), respectively to the anomaly. The time series of FWT and ST anomaly, and the contribution from the different anomaly terms are shown in Figure S4 in the Supporting Information S1.

3.4. Uncertainty Analysis

Before September 2014, the significant data gaps (i.e., lost moorings and instrument failures) especially for the near-surface velocity, resulted in high uncertainty that could reach up to 30% (Figures 9a and 9b). In Figure 9b we show the relative uncertainty time series, while the horizontal lines show the mooring deployments with at least one velocity sampling point above 100m. In the absence of velocity instruments in the upper 100m of the moorings F13 and F14, the uncertainty is higher than 20% for a large period of the year. After September 2014, when the new mooring F13b is included and more instruments are in place (i.e., new ADCPs at the surface and more instruments in the halocline), the uncertainty drops to below 10% and remains low in the absence of major instrumentation loss, for example, the loss of F17 between Sept. 2018–Sept. 2019.

The total uncertainty is largely defined by the uncertainty of gridding. For an estimate of this uncertainty, a single baseline data set (mean of September CTD data) is used for all months (see Section 2.4), thus the seasonality of the gridding uncertainty is not addressed. The seasonality in the total uncertainty originates from the uncertainty at the interpolants (see Text S1 in the Supporting Information S1). Interpolants with data gaps are filled with the long-term mean, or regressed with coefficients from other year deployments (see Section 2.3). Those methods are more precarious for August–September as in those months salinity and velocity are more variable from year to year, resulting in larger uncertainty (Figure 9c). Overall, the uncertainty of FWT is largely dependent on the availability of velocity instruments near the surface. This is because upper ocean velocity is much more variable than salinity in time and space, resulting in high uncertainty when velocity data gaps are regressed or interpolated. We mention that the estimated interpolation uncertainty is dependent on the selection of the baseline data set. In this analysis the mean September CTD data set was used as a baseline, however, a sensitivity analysis with alternative baseline datasets, for example, high-resolution model output, could give additional information.

4. Discussion

Since period 1, the salinity stratification within the Polar Water in the western Fram Strait has increased. This is caused by freshening near the surface where $\sigma_\theta < 26.5$ kg/m^3, and salinification in the layer $26.5 > \sigma_\theta > 27.7$ kg/m^3. This freshening and increasing stratification in the western Fram Strait is coherent with a shrinking ice-cover in the central Arctic Ocean which results in additional freshwater input at the surface through increased melt of sea ice during summer (Onarheim et al., 2018). The increasing salinity in the halocline could be due to enhanced winter-ice formation and brine rejection on the Arctic shelves. However, as it is associated with a

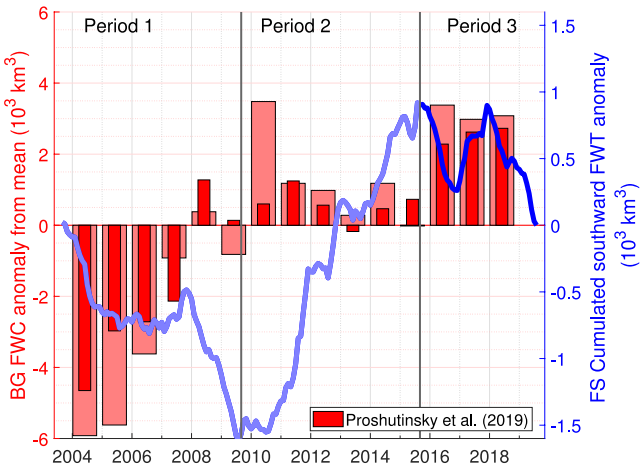

Figure 10. Cumulative southward FWT anomaly in Fram Strait, with respect to the 2003–2019 long-term mean (46.7 mSV), relative to 34.8. Increasing (decreasing) values denote more (less) southward fresh water transport than 46.7 mSV. The blue and pale blue lines show the time series before and after September 2015. The red and pale red bars show the FWC anomaly in the Beaufort Gyre relative to 34.8 from moorings and ITP data presented in Proshutinsky et al. (2019).

shoaling of the 0°C isotherm at the same time, it indicates that the observed weakening of the cold halocline and shoaling of the Atlantic Water in the Eurasian Arctic (Polyakov et al., 2020) is also observed in the Fram Strait, suggesting that the so-called "Atlantification" as described for the Barents Sea (Årthun et al., 2012) and Eurasian Basin (Lind et al., 2018; Polyakov et al., 2017, 2020) is now also occurring in the western Fram Strait.

The "Atlantification" in our observations is demonstrated by the shoaling of the AW and the westward shift of the Polar-Atlantic front (Figures 6g and 6h). In general, the "Atlantification" of the Arctic Ocean, which has been occurring over the last century, denotes a larger presence of AW in the water column, and an increase in heat transport toward the Arctic Ocean (Smedsrud et al., 2021; Steele & Boyd, 1998). At present, it is not clear if the "Atlantification" of the western Fram Strait described here is due to increased AW recirculation north of the mooring array or due to advection from the Eurasian basin. The shoaling of the AW in western Fram Strait occurs gradually since 2003, indicating possibly advection from the Eurasian Basin. However, the westward shift of the Polar-Atlantic front occurred abruptly in June 2015, simultaneously with the reduction in the upper ocean velocity indicating possibly changing forcing over the Fram Strait. Still, the wind-velocity data analyzed here show only a small decreasing trend, while the variability is large. We speculate that in recent years, signatures from upstream processes as well as locally driven changes have emerged in the Arctic outflow in the western Fram Strait, however, the distinction between the two is not clear. The distinct westward move of the Polar-Atlantic front in 2015, as well as the reduced upper ocean transport, is the subject of ongoing research.

Here, we compare the cumulated southward FWT anomaly with respect to its long-term mean (2003–2019) with the FWC anomaly in the Beaufort Gyre (BG) obtained from Proshutinsky et al. (2019), both for a reference salinity of 34.8 (Figure 10). This comparison shows that FW volume anomaly through Fram Strait and the FWC in the BG show opposite trends within the three periods (however the correlation coefficient for annual means is small and not significant). Between 2003 and 2009 (period 1), the FWC of the BG increased while the FWT in the Fram Strait was less than the mean. This coincided with an intensification of the BG (McPhee et al., 2009; Proshutinsky et al., 2009) and a diversion of riverine water from the Siberian shelves to the BG (Morison et al., 2012), which decreased the transport toward Fram Strait. Between 2009 and 2015 (period 2), the FWC increase stabilized during a temporary relaxation of the BG, and an eastward expansion of dynamic ocean topography (De Steur et al., 2013) allowed some freshwater from the BG to move toward Fram Strait leading to increased FWT. In accordance to that, the correlation between the local wind forcing and the volume transport in the western Fram Strait was exceptionally low during this period (Figure 8) confirming that upstream changes were responsible for the increased FWT. After 2015 (period 3), the FWC of the BG generally increased again and the FWT in the Fram Strait decreased.

During periods of intensification of the BG (periods 1 and 3), the FWC in the BG increases and the FWT in the Fram Strait decreases (Figure 10). However, this decrease is only a fraction (between 0.1 and 0.35) of the FWC gain in the BG, reflecting that during periods of intensification, freshwater converges in the BG from a wider area of the Arctic. During period 2, when the BG stabilized, the cumulative increase of FWT in Fram Strait (2.300 km^3) constituted a significant amount of the concurrent freshwater decrease in the BG (3.500 km^3 according to the ITP data), supporting that between 2009 and 2015 nearly 65% of the fresh water released from the BG ended up in Fram Strait. This suggests an important link between the FWC of the BG and the FWC in the Fram Strait.

Since the changes in the FWT of the Fram Strait between the three periods are dominated by changing volume transport (i.e., velocity) of the PW and less by changing FWC (Figures 7b, 7d, and 7f), concurrent dynamical forcing of the two regions may be important as well. Further work is needed on identifying the possible links and driving mechanisms between the FWC of the BG and the FWT in the Fram Strait. This may include possible teleconnections between the sea-level pressure over the BG driving the storage of freshwater, and the wind

forcing over the Fram Strait largely controlling the outflow (De Steur et al., 2018). Additionally, sensitivity experiments with circulation models, as well as analysis of the Arctic dynamic topography over the Fram Strait can be considered.

We anticipate that the FWT anomalies described here have an effect downstream in the Nordic Seas, on the overturning circulation, and even beyond that. This is because ~50% of the Fram Strait FWT is estimated to be transformed into the deep water flowing southward at depth (Le Bras et al., 2021). Moreover, the projected freshening of the central Arctic Ocean (Jahn & Laiho, 2020) suggests that FWT will increase eventually. However, the near-future changes of the FWT in the Fram Strait are not clear yet. Following mostly velocity, the FWT in the Fram Strait experiences high interannual variability, suggesting that near-future projections of the FWT in the Fram Strait can only be speculative. Still, the described relation between the FWC in the BG and the FWT in the Fram Strait may suggest that the future changes of those two variables will continue to be linked.

At present, the FWT on the East Greenland Shelf west of the mooring array remains unknown and provides the largest uncertainty in our total FWT estimate at this latitude. Moreover, it is unclear if the variability of the FWT presented here is indeed due to temporal variations of the EGC or if changing pathways of freshwater contribute. As an example, the current, likely resembling the Polar Surface Jet, that was seen over the shelf break between 2009 and 2015 is not clearly observed after 2015. Still, the current may instead have occurred further west on the shelf, and thus it may not have been captured by the moorings. If conclusions are to be drawn for the total magnitude and variability of the Arctic freshwater outflow in the area, enhanced monitoring of the shelf current system is required. Available and recently obtained summer hydrographic data over the Greenland Shelf are subject to further research including an analysis of seasonality on the shelf.

Finally, we presented the ST of the EGC which is independent of any reference value, addressing the ambiguity of FWC and FWT that depend on a reference salinity (Schauer & Losch, 2019). We found that in the EGC, the ST anomaly is not sensitive to salinity changes, as it is fully determined by the anomaly of velocity. This makes salt transport not suitable to identify salinity variations in the outflow. The independence of ST anomaly on salinity relates to the small value of a typical anomaly to-mean ratio for salinity compared to velocity. Even though the FWT has limitations, it is still an efficient way to quantify and visualize changes in the combined salinity and velocity field and its effects on basin-scale hydrography. This, as the reference salinity in the numerator of the fresh water fraction (Equation 1) decreases the mean value of salinity without decreasing its anomaly from the mean, resulting in a comparable anomaly to-mean ratio for velocity and freshwater fraction. However, we acknowledge that the use of different reference salinities when quantifying FWT and FWC in the literature leads to confusion. We suggest that if ST is preferred, it should be looked at in specific salinity domains, then ST anomaly depends on velocity directly, and on salinity through the limits of integration (Equation 2), without using a reference salinity.

5. Conclusions

Between 2015 and 2019, the fresh water transport (FWT) from the East Greenland Current (EGC) decreased. This was driven by reduced volume transport (VT) and freshwater content (FWC) in the Polar Water (PW: $\sigma_\theta < 27.7$ kg/m^3 & $T < 0$°C), which constitutes 95% of the FWT above the reference level of 34.9. From Sept. 2015 to Aug. 2019, the FWT of the PW reached an average of 59.9 ($\pm$4.5) mSV, 15% less than the long-term mean. The salt transport (ST) anomaly coincides with the VT anomaly, meaning that ST is not sensitive to salinity changes. The average salt transport integrated over the full section between 2015 and 2019, was 260.5 kT/s of which the 42.6 kT/s occurred within the PW layer. Since 2015, both the VT and FWC in the PW experienced a significant decrease. The decreased FWC was related to a strong salinification of the lower halocline ($26.5 < \sigma_\theta < 27.7$ kg/m^3) which counterbalanced the freshening of the top layer ($\sigma_\theta < 26.5$ kg/m^3). Between 2003 and 2019, the results showed significant increase in the salinity stratification of the PW, as the salinity difference between 155 and 55 m increased by 0.63 psu. Moreover, in that period, the PW layer over the shelf became thinner by approximately 40–50 m and the eastward extent of the PW from the shelf break decreased by approximately 10 km in 2015. Finally, the salinification in the lower halocline was stronger over the shelf leading to a smaller tilt of the isopycnals and a weaker geostrophic velocity, which explained 67% of the mean-velocity reduction after 2015.

The long-term mean FWT of the EGC observed with the mooring array, appears not very sensitive to changes of the array's configuration. This means that estimates from previous years with less moored instruments are comparable with recent ones when coverage is higher. However, the newly deployed instruments demonstrate a seasonal bias in the earlier estimates. Salinity sensors (IceCATs) deployed at 25 m depth demonstrate that the FWC is in fact higher during September and October, and lower between November and February compared to the earlier applied estimates. Velocity sensors from the additional mooring F13B at 5.5° W show that VT is smaller in summer, however, the differences are not significant and are within the uncertainty of the earlier estimations. Nevertheless, the improved instrument coverage of the mooring array results in lower uncertainty in the calculation of FWT. The mean uncertainty after 2015 is 8%, significantly smaller than the mean uncertainty of previous years (17%). However, significant uncertainty still relates to the unknown transport over the East Greenland Shelf west of 8°W.

Conflict of Interest

The authors declare no conflicts of interest relevant to this study.

Data Availability Statement

The data are available at: https://data.npolar.no/dataset/8bb85388-327e-4b01-892c-5d1836d44ca4 (Moored current meter data from the western Fram Strait 1997–2009), https://data.npolar.no/dataset/c4d80b64-25f6-4afd-b392-696430c3fd14 (Moored current meter and hydrographic data from the Fram Strait Arctic Outflow Observatory since 2009), https://data.npolar.no/dataset/049178d8-9bd3-42b3-a793-606690a5cd8a (Fram Strait gridded monthly mean velocity and salinity and time-series of fresh water transport, freshwater content, volume transport and salt transport since 2003), and https://cds.climate.copernicus.edu/#!/home (ERA5 wind data downloaded at 23-June-2020).

Acknowledgments
This work was carried out in the FreshArc project supported by the Norwegian Research Council through the FRIPRO program (Grant 286971). We like to thank Kristen Fossan for servicing the moorings and instruments and thanks to all crew of R/V Lance and R/V Kronprins Haakon. We thank Paul A. Dodd for providing processed CTD data and Zoe Koenig for the insightful discussions on the uncertainty analysis. Finally, we thank the three reviewers for their constructive comments that improved the quality of this paper significantly.

References

Aagaard, K., & Carmack, E. (1968). The East Greenland current north of Denmark strait: Part1. *Arctic*, *21*, 181–200. https://doi.org/10.14430/arctic3262

Aagaard, K., & Carmack, E. C. (1989). The role of sea ice and other fresh water in the Arctic circulation. *Journal of Geophysical Research*, *94*(C10), 14485–14498. https://doi.org/10.1029/JC094iC10p14485

Årthun, M., Eldevik, T., Smedsrud, L. H., Skagseth, Ø., & Ingvaldsen, R. B. (2012). Quantifying the influence of atlantic heat on barents sea ice variability and retreat. *Journal of Climate*, *25*(13), 4736–4743. https://doi.org/10.1175/JCLI-D-11-00466.1

Collins, M., Knutti, R., Arblaster, J., Dufresne, J.-L., Fichefet, T., Friedlingstein, P., & Wehner, M., et al. (2013). Chapter 12 - long-term climate change: Projections, commitments and irreversibility. In *Climate change 2013: The physical science basis. ipcc working group i contribution to ar5*. Cambridge University Press. Retrieved from http://pure.iiasa.ac.at/id/eprint/10551/

Curry, B., Lee, C. M., Petrie, B., Moritz, R. E., & Kwok, R. (2014). Multiyear volume, liquid freshwater, and sea ice transports through davis strait, 2004-10. *Journal of Physical Oceanography*, *44*(4), 1244–1266. https://doi.org/10.1175/JPO-D-13-0177.1

De Steur, L., Hansen, E., Gerdes, R., Karcher, M., Fahrbach, E., & Holfort, J. (2009). Freshwater fluxes in the east Greenland current: A decade of observations. *Geophysical Research Letters*, *36*(23). https://doi.org/10.1029/2009GL041278

De Steur, L., Hansen, E., Mauritzen, C., Beszczynska-Möller, A., & Fahrbach, E. (2014). Impact of recirculation on the east Greenland current in Fram Strait: Results from moored current meter measurements between 1997 and 2009. *Deep Sea Research Part I: Oceanographic Research Papers*, *92*, 26–40. https://doi.org/10.1016/j.dsr.2014.05.018

De Steur, L., Peralta-Ferriz, C., & Pavlova, O. (2018). Freshwater export in the east Greenland current freshens the North Atlantic. *Geophysical Research Letters*, *45*(24), 13359–13366. https://doi.org/10.1029/2018GL080207

De Steur, L., Steele, M., Hansen, E., Morison, J., Polyakov, I., Olsen, S. M., et al. (2013). Hydrographic changes in the Lincoln Sea in the Arctic Ocean with focus on an upper ocean freshwater anomaly between 2007 and 2010. *Journal of Geophysical Research: Oceans*, *118*(9), 4699–4715. https://doi.org/10.1002/jgrc.20341

Foukal, N. P., Gelderloos, R., & Pickart, R. S. (2020). A continuous pathway for fresh water along the east Greenland shelf. *Science Advances*, *6*(43), eabc4254. https://doi.org/10.1126/sciadv.abc4254

Giles, K., Laxon, S., & Ridout, A. e. a. (2012). Western Arctic Ocean freshwater storage increased by wind-driven spin-up of the Beaufort Gyre. *Nature Geoscience*, *5*, 194–197. https://doi.org/10.1038/ngeo1379

Graham, R. M., Cohen, L., Petty, A. A., Boisvert, L. N., Rinke, A., Hudson, S. R., & Granskog, M. A. (2017). Increasing frequency and duration of Arctic winter warming events. *Geophysical Research Letters*, *44*(13), 6974–6983. https://doi.org/10.1002/2017GL073395

Haine, T. W. N. (2020). Arctic Ocean freshening linked to anthropogenic climate change: All hands on deck. *Geophysical Research Letters*, *47*(22), e2020GL090678. https://doi.org/10.1029/2020GL090678

Haine, T. W. N., Curry, B., Gerdes, R., Hansen, E., Karcher, M., Lee, C., & Woodgate, R. (2015). Arctic freshwater export: Status, mechanisms, and prospects. *Global and Planetary Change*, *125*, 13–35. https://doi.org/10.1016/j.gloplacha.2014.11.013

Håvik, L., Pickart, R. S., Våge, K., Torres, D., Thurnherr, A. M., Beszczynska-Möller, A., & von Appen, W.-J. (2017). Evolution of the east Greenland current from fram strait to Denmark strait: Synoptic measurements from summer 2012. *Journal of Geophysical Research: Oceans*, *122*(3), 1974–1994. https://doi.org/10.1002/2016JC012228

Hersbach, H., Bell, B., Berrisford, P., Hirahara, S., Horányi, A., Muñoz-Sabater, J., & Thépaut, J.-N. (2020). The era5 global reanalysis. *Quarterly Journal of the Royal Meteorological Society*, *146*(730), 1999–2049. https://doi.org/10.1002/qj.3803

Heuzé, C. (2017). North Atlantic deep water formation and AMOC in CMIP5 models. *Ocean Science*, *13*(4), 609–622. https://doi.org/10.5194/os-13-609-2017

Holfort, J., & Meincke, J. (2005). Time series of freshwater-transport on the east Greenland shelf at 74N. *Meteorologische Zeitschrift*, *14*(6), 703–710. https://doi.org/10.1127/0941-2948/2005/0079

Jahn, A., & Laiho, R. (2020). Forced changes in the arctic freshwater budget emerge in the early 21st century. *Geophysical Research Letters*, *47*(15), e2020GL088854. https://doi.org/10.1029/2020GL088854

Le Bras, I., Straneo, F., Muilwijk, M., Smedsrud, L. H., Li, F., Lozier, M. S., & Holliday, N. P. (2021). How much arctic fresh water participates in the subpolar overturning circulation? *Journal of Physical Oceanography*, *51*(3), 955–973. https://doi.org/10.1175/JPO-D-20-0240.1

Lind, S., Ingvaldsen, R., & Furevik, T. (2018). Arctic warming hotspot in the northern Barents Sea linked to declining sea-ice import. *Nature Climate Change*, *8*, 634–639. https://doi.org/10.1038/s41558-018-0205-y

Lique, C., Holland, M. M., Dibike, Y. B., Lawrence, D. M., & Screen, J. A. (2016). Modeling the Arctic freshwater system and its integration in the global system: Lessons learned and future challenges. *Journal of Geophysical Research: Biogeosciences*, *121*(3), 540–566. https://doi.org/10.1002/2015JG003120

Lobelle, D., Beaulieu, C., Livina, V., Sévellec, F., & Frajka-Williams, E. (2020). Detectability of an AMOC decline in current and projected climate changes. *Geophysical Research Letters*, *47*(20), e2020GL089974. https://doi.org/10.1029/2020GL089974

Marnela, M., Rudels, B., Goszczko, I., Beszczynska-Möller, A., & Schauer, U. (2016). Fram Strait and Greenland Sea transports, water masses, and water mass transformations 1999-2010 (and beyond). *Journal of Geophysical Research: Oceans*, *121*(4), 2314–2346. https://doi.org/10.1002/2015JC011312

McPhee, M. G., Proshutinsky, A., Morison, J. H., Steele, M., & Alkire, M. B. (2009). Rapid change in freshwater content of the Arctic Ocean. *Geophysical Research Letters*, *36*(10). https://doi.org/10.1029/2009GL037525

Moore, G. W. K., Schweiger, A., Zhang, J., & Steele, M. (2018). Collapse of the 2017 winter Beaufort high: A response to thinning sea ice? *Geophysical Research Letters*, *45*(6), 2860–2869. https://doi.org/10.1002/2017GL076446

Morison, J., Kwok, R., Peralta-Ferriz, C., Alkire, M., Rigor, I., Andersen, R., & Steele, M. (2012). Changing Arctic Ocean freshwater pathways. *Journal of Geophysical Research*, *481*(70). https://doi.org/10.1038/nature10705

Mosby, H. (1962). Water, salt, and heat balance of the Polar Ocean, with special emphasis on the Fram Strait. *Norsk Polarinstitutt Skrifter*, *188*, 1–53.

Onarheim, I. H., Eldevik, T., Smedsrud, L. H., & Stroeve, J. C. (2018). Seasonal and regional manifestation of arctic sea ice loss. *Journal of Climate*, *31*(12), 4917–4932. https://doi.org/10.1175/JCLI-D-17-0427.1

Polyakov, I., Pnyushkov, A., Alkire, M., Ashik, I., Baumann, T., Carmack, E., et al. (2017). Greater role for atlantic inflows on sea-ice loss in the Eurasian Basin of the Arctic Ocean. *Science*, *356*, 285–291. https://doi.org/10.1126/science.aai8204

Polyakov, I., Rippeth, T. P., Fer, I., Alkire, M. B., Baumann, T. M., Carmack, E. C., et al. (2020). Weakening of cold halocline layer exposes sea ice to oceanic heat in the eastern Arctic Ocean. *Journal of Climate*, *33*(18), 8107–8123. https://doi.org/10.1175/JCLI-D-19-0976.1

Proshutinsky, A., Krishfield, R., Timmermans, M.-L., Toole, J., Carmack, E., McLaughlin, F., et al. (2009). Beaufort Gyre freshwater reservoir: State and variability from observations. *Journal of Geophysical Research: Oceans*, *114*(C1). https://doi.org/10.1029/2008JC005104

Proshutinsky, A., Krishfield, R., Toole, J. M., Timmermans, M.-L., Williams, W., Zimmermann, S., et al. (2019). Analysis of the Beaufort gyre freshwater content in 2003-2018. *Journal of Geophysical Research: Oceans*, *124*(12), 9658–9689. https://doi.org/10.1029/2019JC015281

Quadfasel, D., Gascard, J.-C., & Koltermann, K.-P. (1987). Large-scale oceanography in Fram Strait during the 1984 marginal ice zone experiment. *Journal of Geophysical Research*, *92*(C7), 6719–6728. https://doi.org/10.1029/JC092iC07p06719

Rabe, B., Dodd, P. A., Hansen, E., Falck, E., Schauer, U., Mackensen, A., et al. (2013). Liquid export of arctic freshwater components through the Fram Strait 1998-2011. *Ocean Science*, *9*(1), 91–109. https://doi.org/10.5194/os-9-91-2013

Rabe, B., Karcher, M., Kauker, F., Schauer, U., Toole, J. M., Krishfield, R. A., et al. (2014). Arctic Ocean basin liquid freshwater storage trend 1992-2012. *Geophysical Research Letters*, *41*(3), 961–968. https://doi.org/10.1002/2013GL058121

Rudels, B. (2009). Arctic Ocean circulation. In J. Steel, K. K. Turekian & S. Thorp (Eds.), *Encyclopedia of ocean science*. Academic Press. https://doi.org/10.1016/b978-012374473-9.00601-9

Rudels, B., Björk, G., Nilsson, J., Winsor, P., Lake, I., & Nohr, C. (2005). The interaction between waters from the Arctic Ocean and the Nordic seas north of Fram Strait and along the east Greenland current: Results from the Arctic Ocean-02 oden expedition. *Journal of Marine Systems*, *55*(1), 1–30. https://doi.org/10.1016/j.jmarsys.2004.06.008

Schauer, U., & Losch, M. (2019). "Freshwater" in the ocean is not a useful parameter in climate research. *Journal of Physical Oceanography*, *49*(9), 2309–2321. https://doi.org/10.1175/JPO-D-19-0102.1

Shu, Q., Qiao, F., Song, Z., Zhao, J., & Li, X. (2018). Projected freshening of the Arctic Ocean in the 21st century. *Journal of Geophysical Research: Oceans*, *123*(12), 9232–9244. https://doi.org/10.1029/2018JC014036

Smedsrud, L. H., Muilwijk, M., Brakstad, A., Madonna, E., Lauvset, S. K., Spensberger, C., et al. (2021). Nordic seas heat loss, atlantic inflow, and arctic sea ice cover over the last century. *Reviews of Geophysics*, *59*, e2020RG000725. https://doi.org/10.1029/2020RG000725

Spreen, G., de Steur, L., Divine, D., Gerland, S., Hansen, E., & Kwok, R. (2020). Arctic sea ice volume export through fram strait from 1992 to 2014. *Journal of Geophysical Research: Oceans*, *125*(6), e2019JC016039. https://doi.org/10.1029/2019JC016039

Steele, M., & Boyd, T. (1998). Retreat of the cold halocline layer in the arctic ocean. *Journal of Geophysical Research: Oceans*, *103*(C5), 10419–10435. https://doi.org/10.1029/98JC00580

Stommel, H. (1961). Thermohaline convection with two stable regimes of flow. *Tellus*, *13*(2), 224–230. https://doi.org/10.3402/tellusa.v13i2.9491

Zhang, J., Steele, M., Runciman, K., Dewey, S., Morison, J., Lee, C., et al. (2016). The Beaufort gyre intensification and stabilization: A model-observation synthesis. *Journal of Geophysical Research: Oceans*, *121*(11), 7933–7952. https://doi.org/10.1002/2016JC012196